

The Paschos-Wolfenstein relation in a hadronic picture

C. Praet,* N. Jachowicz,[†] J. Ryckebusch, P. Vancraeyveld, and K. Vantournhout

Department of Subatomic and Radiation Physics,

Ghent University,

Proeftuinstraat 86,

B-9000 Gent, Belgium.

(Dated: July 31, 2018)

Abstract

The Paschos-Wolfenstein (PW) relation joins neutral- and charged-current neutrino- and antineutrino-induced cross sections into an expression that depends on the weak mixing angle $\sin^2 \theta_W$. Contrary to the traditional approach with partonic degrees of freedom, we adopt a model built on hadronic degrees of freedom to perform a study of the PW relation at intermediate neutrino energies (100 MeV - 2 GeV). With upcoming high-statistics scattering experiments like MINER ν A and FINeSSE, a scrutiny of the PW relation is timely. Employing a relativistic Glauber nucleon knockout model for the description of quasi-elastic neutrino-nucleus reactions, the influence of nuclear effects on the PW relation is investigated. We discuss nuclear model dependences and show that the PW relation is a robust ratio, mitigating the effect of final-state interactions, for example, to the 1% level. The role played by a possible strangeness content of the nucleon is investigated. It appears that the uncertainties arising from the poorly known strangeness parameters and the difficulties in nuclear modelling seriously limit the applicability of the PW relation as an intermediate-energy electroweak precision tool. On the other hand, we show that nuclear effects may be sufficiently well under control to allow the extraction of new information on the axial strangeness parameter. Results are presented for ^{16}O and ^{56}Fe .

PACS numbers: 25.30.Pt,13.88.+e,24.70.+s,13.15.+g

*Electronic address: christophe.praet@UGent.be

[†]Electronic address: natalie.jachowicz@UGent.be

I. INTRODUCTION

Now more than ever, neutrinos are valued for their wide probing potential in many different domains. At intermediate energies, they are put forward to study nucleon structure and probe nuclear effects [1]. Well-defined ratios of neutrino-scattering cross sections prove being promising tools to measure the strange-quark contribution to the nucleon spin [2, 3]. Lately, neutrinos have been regarded as interesting candidates for electroweak tests aiming at a precision measurement of the Weinberg angle θ_W [4, 5, 6].

One of the most fundamental parameters in the standard model (SM), the weak mixing angle has been at the center of research activities, involving both theoretical SM calculations [7, 8] and experimental efforts to determine its value. While all $\sin^2 \theta_W$ measurements near the Z^0 pole [9, 10] and for low Q^2 values [11, 12] are in good agreement with the SM prediction, an experiment by the NuTeV collaboration at $Q^2 = 20 \text{ GeV}^2$ does not seem to corroborate the calculated running of the Weinberg angle [4]. Explanations for this anomalous result range from quantum chromodynamics (QCD) uncertainties [13, 14], to nuclear effects [15, 16] and even interpretations involving new physics [17, 18]. Whether the surprising NuTeV outcome can be resolved through a further analysis of the data or indeed hints at new physics beyond the SM, is up to this day an unresolved issue [19]. In NuTeV's analysis, the Paschos-Wolfenstein relation [20] plays an essential role in relating the weak mixing angle to measured ratios of neutral-current (NC) to charged-current (CC) deep-inelastic scattering (DIS) neutrino cross sections. As a consequence, it has been tested very well in the DIS regime with respect to genuine QCD mechanisms. To the contrary, little effort has been put in the intermediate-energy regime, where an adequate description in terms of hadronic rather than partonic degrees of freedom is needed.

In this work, we explore what physics could be probed by future measurements of the Paschos-Wolfenstein relation at medium energies. With newly proposed, high-precision neutrino-scattering experiments like MINER ν A [1] and FINeSSE [3], it is timely to make predictions about the level of sensitivity one would need to extract relevant physics from these measurements. As a matter of fact, the MINER ν A proposal contains an extensive program for studying nuclear effects with neutrinos [21]. More specifically, the impact of the nuclear medium on NC/CC cross-section ratios will be investigated by employing carbon, iron and lead target nuclei. In this paper, we focus on a study of the PW relation in the

few GeV regime, adopting a model based on hadronic degrees of freedom [22]. Considering quasi-elastic (QE) neutrino-nucleus scattering with nucleon knockout as the basic source of strength in the 100 MeV - 2 GeV energy range, the PW relation is constructed for both oxygen and iron target nuclei. Treating nucleon-nucleon interactions in a relativistic mean-field approximation, binding effects and the Pauli exclusion principle are naturally included in our approach. Final-state interactions of the outgoing nucleon are incorporated through a Glauber approach. Within this model, we show how the nuclear medium affects the PW relation. A model-dependence discussion is included in this work, by comparing predictions within different frameworks.

Knowing at what level nuclear uncertainties affect the PW relation, one can proceed with putting theoretical constraints on the accuracy with which variables can be determined from it. In earlier work by Donnelly and Musolf [23], nuclear uncertainties were estimated too large to allow a $\sin^2 \theta_W$ determination in parity-violating electron scattering (PVES) with a precision similar to other types of measurements. It is important to check if the PW relation at medium energies provides a powerful tool for a Weinberg-angle extraction in the QE regime. In addition, the Paschos-Wolfenstein relation has been suggested to serve as a lever for the determination of the strange-quark contribution to the nucleon's spin, g_A^s [24, 25]. This and other work [26, 27, 28] points out that for sufficiently high energies (~ 1 GeV), ratios of neutrino cross sections can serve as theoretically clean probes for the nucleon's strangeness content. Here, we derive a theoretical error bar for g_A^s as extracted from the PW relation. Given that the PW relation is both sensitive to the weak mixing angle and the strangeness content of the nucleon, it is worthwhile to conduct a study of how these parameters are intertwined. This type of study is surely relevant for the future FINeSSE experiment, which aims at measuring the ratios of NC to CC neutrino-induced cross sections at medium energies to extract information on the strange axial form factor g_A^s .

The paper is organized as follows. Section II introduces the Paschos-Wolfenstein relation in its traditional, DIS form. The third section discusses the theoretical framework used in this paper for the description of neutrino-nucleus interactions. An analytical estimate of the Paschos-Wolfenstein ratio for intermediate-energy neutrino-nucleus scattering reactions is derived in section IV. Numerical results are presented in section V. Our conclusions are summarized in section VI.

II. THE PASCHOS-WOLFENSTEIN RELATION

Traditionally, the Paschos-Wolfenstein relation is defined as the following ratio of NC to CC (anti)neutrino-nucleon cross sections

$$\text{PW} = \frac{\sigma^{\text{NC}}(\nu N) - \sigma^{\text{NC}}(\bar{\nu} N)}{\sigma^{\text{CC}}(\nu N) - \sigma^{\text{CC}}(\bar{\nu} N)}. \quad (1)$$

Adopting the nucleon's quark-parton structure, the PW relation can be computed starting from the quark currents

$$\begin{aligned} \hat{j}_\mu^{(Z)} &= \sum_{q=u,d} g_{q,L} \bar{q} \gamma_\mu (1 - \gamma_5) q + g_{q,R} \bar{q} \gamma_\mu (1 + \gamma_5) q \quad \text{NC}, \\ \hat{j}_\mu^{(+)} &= \frac{1}{2} \bar{u} \gamma_\mu (1 - \gamma_5) d, \quad \hat{j}_\mu^{(-)} = \frac{1}{2} \bar{d} \gamma_\mu (1 - \gamma_5) u \quad \text{CC}, \end{aligned} \quad (2)$$

with the quark coupling strengths

$$\begin{aligned} g_{u,L} &= \frac{1}{2} - \frac{2}{3} \sin^2 \theta_W, & g_{u,R} &= -\frac{2}{3} \sin^2 \theta_W, \\ g_{d,L} &= -\frac{1}{2} + \frac{1}{3} \sin^2 \theta_W, & g_{d,R} &= \frac{1}{3} \sin^2 \theta_W. \end{aligned} \quad (3)$$

Using these expressions, one immediately derives [29]

$$\text{PW} = \left(\frac{1}{\cos^2 \theta_c} \right) \left(\frac{1}{2} - \sin^2 \theta_W \right), \quad (4)$$

where θ_c stands for the Cabibbo mixing angle. Equation (4) holds for isoscalar targets, containing an equal number of u and d quarks, and neglecting s quarks.

III. CROSS SECTIONS FOR QUASI-ELASTIC NEUTRINO-NUCLEUS INTERACTIONS

A description in terms of quark currents is no longer appropriate when considering neutrino-nucleus interactions at medium energies. Instead, one usually invokes form factors to map the nucleon's substructure. With these form factors, matrix elements of the hadronic current are constructed based on general principles of Lorentz invariance. In this section, the formalism employed for the calculation of neutrino-nucleus cross sections is pre-

sented. We consider quasi-elastic (anti)neutrino-nucleus interactions of the following type

$$\begin{aligned}
\nu + A &\xrightarrow{\text{NC}} \nu + (A - 1) + N, \\
\bar{\nu} + A &\xrightarrow{\text{NC}} \bar{\nu} + (A - 1) + N, \\
\nu + A &\xrightarrow{\text{CC}} l^- + (A - 1) + p, \\
\bar{\nu} + A &\xrightarrow{\text{CC}} l^+ + (A - 1) + n,
\end{aligned} \tag{5}$$

limiting ourselves to processes where the final nucleus $(A - 1)$ is left with an excitation energy not exceeding a few tens of MeV. The target nucleus is denoted by its mass number A , l represents an outgoing charged lepton and N stands for the ejectile (proton p or neutron n). To calculate the corresponding cross sections, we turn to the relativistic quasi-elastic nucleon knockout model described in [22]. Writing $K'^{\mu} = (\epsilon', \vec{k}')$, $K_N^{\mu} = (\epsilon_N, \vec{k}_N)$ and $K_{A-1}^{\mu} = (\epsilon_{A-1}, \vec{k}_{A-1})$ for the four-momenta of the scattered lepton, the ejectile and the residual nucleus, these cross sections are given by

$$\frac{d^5\sigma}{d\epsilon'd^2\Omega_l d^2\Omega_N} = \frac{M_l M_N M_{A-1}}{(2\pi)^5 \epsilon'} k'^2 k_N f_{rec}^{-1} \overline{\sum_{if}} |M_{fi}|^2. \tag{6}$$

The exclusive cross section (6) still depends on the solid angles Ω_l and Ω_N , determining the direction of the scattered lepton and ejectile respectively. The hadronic recoil factor f_{rec} is given by

$$f_{rec} = \left| \epsilon_{A-1} + \epsilon_N \left(1 - \frac{\vec{q} \cdot \vec{k}_N}{k_N^2} \right) \right|. \tag{7}$$

Further on, an appropriate averaging over initial states and sum over final states is performed in the squared invariant matrix element $|M_{fi}|^2$. Using the Feynman rules, one finds

$$|M_{fi}|^2 = \frac{g^4}{64 \frac{M_W^4}{M_{Z,W}^2} (Q^2 + M_{Z,W}^2)^2} l_{\alpha\beta} W^{\alpha\beta}, \tag{8}$$

with g the weak coupling strength and $Q^2 = -q_{\mu}q^{\mu}$ the four-momentum transfer. For NC (CC) interactions, the boson mass M_Z (M_W) is selected. In the CC case, the right-hand side of (8) should also be multiplied by $\cos^2 \theta_c$. One further distinguishes a lepton part described by the tensor $l_{\alpha\beta}$ and a nuclear part, described by the tensor

$$W^{\alpha\beta} = (\mathcal{J}^{\alpha})^{\dagger} \mathcal{J}^{\beta}. \tag{9}$$

To evaluate the nuclear current matrix elements \mathcal{J}^{μ} , we assume that the major fraction of the transferred energy is carried by the ejectile, thereby neglecting processes that involve

several target nucleons. In the impulse approximation (IA), the nuclear many-body current operator is replaced by a sum of one-body current operators \hat{J}^μ

$$\sum_{k=1}^A \hat{J}^\mu(\vec{r}_k). \quad (10)$$

Employing an independent-particle model (IPM) for the initial and final nuclear wave functions, the current matrix elements can be written as [22]

$$\mathcal{J}^\mu = \int d\vec{r} \bar{\phi}_F(\vec{r}) \hat{J}^\mu(\vec{r}) e^{i\vec{q}\cdot\vec{r}} \phi_B(\vec{r}), \quad (11)$$

where ϕ_B and ϕ_F are relativistic bound-state and scattering wave functions. We adopt the following expression for the weak one-nucleon current operator

$$\begin{aligned} \hat{J}^\mu = & F_1(Q^2)\gamma^\mu + \frac{i}{2M_N}F_2(Q^2)\sigma^{\mu\nu}q_\nu \\ & + G_A(Q^2)\gamma^\mu\gamma_5 + \frac{1}{2M_N}G_P(Q^2)q^\mu\gamma_5, \end{aligned} \quad (12)$$

composed of a vector part, described by the Dirac and Pauli form factors F_1 and F_2 , and an axial part, described by the axial form factor G_A and pseudoscalar form factor G_P . As pointed out for example in [22], one can choose amongst different options for the one-body vertex function, of which (12) is labeled *cc2*. For bound nucleons these parameterizations do not produce identical results, giving rise to the so-called Gordon ambiguity. For the vector form factors two different parameterizations will be considered: a standard dipole form and the BBA parameterization of Ref. [30]. The axial form factor G_A will be parameterized by a dipole. Using the Goldberger-Treiman relation, the pseudoscalar form factor can be related to the axial one

$$G_P(Q^2) = \frac{2M_N}{Q^2 + m_\pi^2} G_A(Q^2), \quad (13)$$

with m_π the pion mass. As the contribution of G_P to the cross section is proportional to the scattered lepton's mass, it vanishes for NC reactions. At $Q^2 = 0$, the form-factor values are given by

$$G_A = \begin{cases} \frac{-g_A\tau_3 + g_A^s}{2} & \text{NC} \\ g_A\tau_\pm & \text{CC} \end{cases} \quad (14)$$

and

$$F_i = \begin{cases} \left(\frac{1}{2} - \sin^2 \theta_W \right) F_i^{EM,V} \tau_3 \\ - \sin^2 \theta_W F_i^{EM,S} - \frac{1}{2} F_i^s & \text{NC} \\ F_i^{EM,V} \tau_{\pm} & \text{CC,} \end{cases} \quad (15)$$

where the superscript s refers to strangeness contributions, $g_A = 1.262$ and the isospin operators are defined in the standard way as

$$\begin{aligned} \tau_3 |p\rangle &= +|p\rangle, & \tau_3 |n\rangle &= -|n\rangle, \\ \tau_+ |n\rangle &= +|p\rangle, & \tau_+ |p\rangle &= 0, \\ \tau_- |p\rangle &= -|n\rangle, & \tau_- |n\rangle &= 0. \end{aligned} \quad (16)$$

The relation between the weak vector form factors and the electromagnetic isovector $F_i^{EM,V} = F_{i,p}^{EM} - F_{i,n}^{EM}$ and isoscalar $F_i^{EM,S} = F_{i,p}^{EM} + F_{i,n}^{EM}$ ones is established by the conserved vector-current (CVC) hypothesis.

Combining terms into longitudinal, transverse and interference contributions, the cross section for NC interactions in Eq. (6) can be written as

$$\begin{aligned} \frac{d^5 \sigma}{d\epsilon' d^2 \Omega_l d^2 \Omega_N} &= \frac{M_N M_{A-1}}{(2\pi)^3} k_N f_{rec}^{-1} \sigma^Z [v_L R_L + v_T R_T \\ &+ v_{TT} R_{TT} \cos 2\phi + v_{TL} R_{TL} \cos \phi \\ &\pm (v'_T R'_T + v'_{TL} R'_{TL} \cos \phi)], \end{aligned} \quad (17)$$

where the upper (lower) sign relates to antineutrino (neutrino) cross sections. We use the notation

$$\sigma^Z = \left(\frac{G_F \cos(\theta_l/2) \epsilon' M_Z^2}{\sqrt{2}\pi(Q^2 + M_Z^2)} \right)^2, \quad (18)$$

and the definitions of Table I. The lepton scattering angle is denoted by θ_l , whereas ϕ stands for the azimuthal angle between the lepton scattering plane and the hadronic reaction plane, defined by \vec{k}_N and \vec{q} . Due to the non-vanishing mass of the outgoing lepton, CC processes imply expressions that are slightly more involved. The expressions for the kinematic factors and response functions are listed in the lower part of Table I. Furthermore, σ^Z has to be replaced by σ^{W^\pm} where

$$\sigma^{W^\pm} = \left(\frac{G_F \cos(\theta_c) \epsilon' M_W^2}{2\pi(Q^2 + M_W^2)} \right)^2 \zeta, \quad \zeta = \sqrt{1 - \frac{M_l^2}{\epsilon'^2}}. \quad (19)$$

TABLE I: Kinematic factors and response functions for NC and CC (anti)neutrino-nucleus scattering. Hadronic matrix elements are expressed in the spherical basis \vec{e}_z , $\vec{e}_{\pm 1} = \mp \frac{1}{\sqrt{2}}(\vec{e}_x \pm i\vec{e}_y)$, $\mathcal{J}^\mu = (\mathcal{J}^0, \vec{\mathcal{J}})$ with $\vec{\mathcal{J}} = -\mathcal{J}^{-1}\vec{e}_{+1} - \mathcal{J}^{+1}\vec{e}_{-1} + \mathcal{J}^z\vec{e}_z$. For the CC case, we only list those expressions that differ from the NC ones.

Kinematic factors	Response functions
<i>Neutral current</i>	
$v_L = 1$	$R_L = \left \mathcal{J}^0 - \frac{\omega}{q} \mathcal{J}^z \right ^2$
$v_T = \tan^2 \frac{\theta_l}{2} + \frac{Q^2}{2q^2}$	$R_T = \mathcal{J}^{+1} ^2 + \mathcal{J}^{-1} ^2$
$v_{TT} = -\frac{Q^2}{2q^2}$	$R_{TT} \cos 2\phi = 2\Re((\mathcal{J}^{+1})^\dagger \mathcal{J}^{-1})$
$v_{TL} = -\frac{1}{\sqrt{2}} \sqrt{\tan^2 \frac{\theta_l}{2} + \frac{Q^2}{q^2}}$	$R_{TL} \cos \phi = -2\Re\left(\mathcal{J}^0 - \frac{\omega}{q} \mathcal{J}^z\right) (\mathcal{J}^{+1} - \mathcal{J}^{-1})^\dagger$
$v'_T = \tan \frac{\theta_l}{2} \sqrt{\tan^2 \frac{\theta_l}{2} + \frac{Q^2}{q^2}}$	$R'_T = \mathcal{J}^{+1} ^2 - \mathcal{J}^{-1} ^2$
$v'_{TL} = \frac{1}{\sqrt{2}} \tan \frac{\theta_l}{2}$	$R'_{TL} \cos \phi = -2\Re\left(\mathcal{J}^0 - \frac{\omega}{q} \mathcal{J}^z\right) (\mathcal{J}^{+1} + \mathcal{J}^{-1})^\dagger$
<i>Charged current</i>	
$v_L R_L = (1 + \zeta \cos \theta_l) \mathcal{J}^0 ^2 + \left(1 + \zeta \cos \theta_l - \frac{2\epsilon\epsilon'}{q^2} \zeta^2 \sin^2 \theta_l\right) \mathcal{J}^z ^2$	
$\quad - \left(\frac{\omega}{q} (1 + \zeta \cos \theta_l) + \frac{M_l^2}{\epsilon'q}\right) 2\Re(\mathcal{J}^0 (\mathcal{J}^z)^\dagger)$	
$v_T = 1 - \zeta \cos \theta_l + \frac{\epsilon\epsilon'}{q^2} \zeta^2 \sin^2 \theta_l$	
$v_{TT} = -\frac{\epsilon\epsilon'}{q^2} \zeta^2 \sin^2 \theta_l$	
$v_{TL} R_{TL} \cos \phi = \frac{\sin \theta_l}{\sqrt{2}q} (\epsilon + \epsilon') \left(2\Re\left(\left(\mathcal{J}^0 - \frac{\omega}{q} \mathcal{J}^z\right) (\mathcal{J}^{+1} - \mathcal{J}^{-1})^\dagger - \frac{M_l^2}{q} \mathcal{J}^z (\mathcal{J}^{+1} - \mathcal{J}^{-1})^\dagger\right)\right)$	
$v'_T = \frac{\epsilon + \epsilon'}{q} (1 - \zeta \cos \theta_l) - \frac{M_l^2}{\epsilon'q}$	
$v'_{TL} = -\frac{\sin \theta_l}{\sqrt{2}} \zeta$	

Final-state interactions (FSI) of the ejectile with the residual nucleus are taken into account by means of a relativistic multiple-scattering Glauber approximation (RMSGGA). In this approach, the scattering wave function of the outgoing nucleon takes on the form

$$\phi_F(\vec{r}) = G(\vec{b}, z) \phi_{k_N, s_N}(\vec{r}), \quad (20)$$

where ϕ_{k_N, s_N} is a relativistic plane wave and $G(\vec{b}, z)$ represents the scalar Dirac-Glauber phase. As a multiple-scattering extension of the eikonal approximation, the Glauber approach describes the emission of a fast nucleon from a composite system of $A - 1$ temporarily frozen nucleons. Details about the RMSGGA approach can be found in Ref. [31]. When FSI

are neglected, $G(\vec{b}, z)$ is put equal to 1, which corresponds to the relativistic plane-wave impulse approximation (RPWIA).

IV. PASCHOS-WOLFENSTEIN RELATION IN NEUTRINO-NUCLEUS SCATTERING

The cross sections in Eq. (17) constitute the ingredients for our study of the PW relation with hadronic degrees of freedom:

$$\text{PW} = \frac{\sigma^{NC}(\nu A) - \sigma^{NC}(\bar{\nu} A)}{\sigma^{CC}(\nu A) - \sigma^{CC}(\bar{\nu} A)}. \quad (21)$$

A numerical calculation of the PW relation can now be performed to investigate its behavior with respect to Eq. (4) and show its sensitivity to various nuclear effects in the intermediate-energy range. Before doing so, however, it is interesting to investigate whether the $\sin^2 \theta_W$ dependence of Eq. (4) can be retrieved within a hadronic picture. First, for inclusive neutrino-scattering reactions, an integration over all angles Ω_l, Ω_N is performed in Eq. (17), thereby nullifying all ϕ -dependent terms. Moreover, ignoring the small differences between proton and neutron wave functions when evaluating the difference of ν - and $\bar{\nu}$ -induced cross sections, we retain only the contribution from the transverse R'_T response. Obviously, for NC processes, this contribution has to be considered for protons and neutrons separately, whereas in the denominator, the charge-exchange feature of the interaction forces neutrinos to interact with neutrons and antineutrinos with protons. Expressing the differential cross sections in terms of the outgoing nucleon's kinetic energy T_N , we obtain for an isoscalar nucleus

$$\begin{aligned} & \frac{\frac{d\sigma^{NC}(\nu A)}{dT_N} - \frac{d\sigma^{NC}(\bar{\nu} A)}{dT_N}}{\frac{d\sigma^{CC}(\nu A)}{dT_N} - \frac{d\sigma^{CC}(\bar{\nu} A)}{dT_N}} \approx \left(\frac{1}{\cos^2 \theta_c} \right) \\ & \times \frac{\sum_{\tau_3=\pm 1} \sum_{\alpha} \int_0^{\pi} \sin \theta_l \sin^2 \frac{\theta_l}{2} d\theta_l \int_0^{\pi} \sin \theta_N d\theta_N k_N f_{rec}^{-1} \frac{dT_N}{d\epsilon'} \frac{\epsilon'^2 M_Z^4}{(4\epsilon\epsilon' \sin^2 \frac{\theta_l}{2} + M_Z^2)^2} \frac{\epsilon + \epsilon'}{q} (R'_T)^{NC}}{\sum_{\alpha} \int_0^{\pi} \sin \theta_l \sin^2 \frac{\theta_l}{2} d\theta_l \int_0^{\pi} \sin \theta_N d\theta_N k_N f_{rec}^{-1} \frac{dT_N}{d\epsilon'} \frac{\epsilon'^2 M_W^4}{(4\epsilon\epsilon' \sin^2 \frac{\theta_l}{2} + M_W^2)^2} \frac{\epsilon + \epsilon'}{q} (R'_T)^{CC}}, \end{aligned} \quad (22)$$

where the summation over α extends over all bound proton single-particle levels in the target nucleus. Furthermore, the mass of the outgoing lepton has been neglected in Eq. (22).

Clearly, the main difference between numerator and denominator lies in the value of the remaining transverse response function R'_T , proportional to $G_A(Q^2)G_M(Q^2)$ with $G_M = F_1 + F_2$ the magnetic Sachs form factor. Assuming that $Q^2 \ll M_Z^2, M_W^2$ and disregarding differences in the contributions of different shells, the expressions in numerator and denominator cancel to a large extent. In other words, the PW relation is approximately given by

$$\begin{aligned} \frac{\frac{d\sigma^{NC}(\nu A)}{dT_N} - \frac{d\sigma^{NC}(\bar{\nu} A)}{dT_N}}{\frac{d\sigma^{CC}(\nu A)}{dT_N} - \frac{d\sigma^{CC}(\bar{\nu} A)}{dT_N}} &\approx \left(\frac{1}{\cos^2 \theta_c} \right) \frac{\sum_{\tau_3=\pm 1} G_A^{NC}(0)G_M^{NC}(0)}{G_A^{CC}(0)G_M^{CC}(0)} \\ &= \left(\frac{1}{\cos^2 \theta_c} \right) \left(\frac{1}{2} - \sin^2 \theta_W \right) + \frac{g_A^s}{g_A} \left(\frac{\sin^2 \theta_W (\mu_p + \mu_n) + \frac{1}{2}\mu_s}{(\mu_p - \mu_n)} \right). \end{aligned} \quad (23)$$

Apart from the standard value figuring in Eq. (4), an additional strangeness term appears. In (23), $\mu_p = F_{2,p}^{EM}(0)$ ($\mu_n = F_{2,n}^{EM}(0)$) denotes the proton (neutron) magnetic moment and $\mu_s = F_2^s(0)$ is the strangeness magnetic moment. We wish to stress that the left-hand side of Eq. (23) is T_N independent.

V. RESULTS AND DISCUSSION

In the previous section, the DIS expression of the PW relation was regained by making various approximations to our hadronic picture. Next, we will evaluate numerically to what extent the nuclear medium affects this *standard value* of the PW relation. To this end, the previously neglected nuclear effects are gradually included and the resulting PW curves are compared with the expression (23). First, the strangeness content of the nucleon will be ignored, putting $g_A^s = 0$ and $\mu_s = 0$. A discussion of the strangeness sensitivity of the PW relation is postponed to subsection V E. Results will be presented for ν_e ($\bar{\nu}_e$) scattering off both an isoscalar nucleus, ^{16}O , and a heavier one, ^{56}Fe , with neutron excess. As a starting point, we use dipole vector and axial form factors, the *cc2* form for the one-nucleon current and an on-shell weak mixing angle $\sin^2 \theta_W = 0.2224$.

A. Relativistic plane-wave impulse approximation

Ignoring FSI of the ejectile with the residual nucleus, we adopt the relativistic plane-wave impulse approximation (RPWIA). Figure 1 displays the PW relation against the outgoing

nucleon's kinetic energy T_N for an incoming neutrino energy of 1 GeV and an ^{16}O target nucleus. Clearly, the $1p_{1/2}$ -shell contribution to the PW relation can not be distinguished

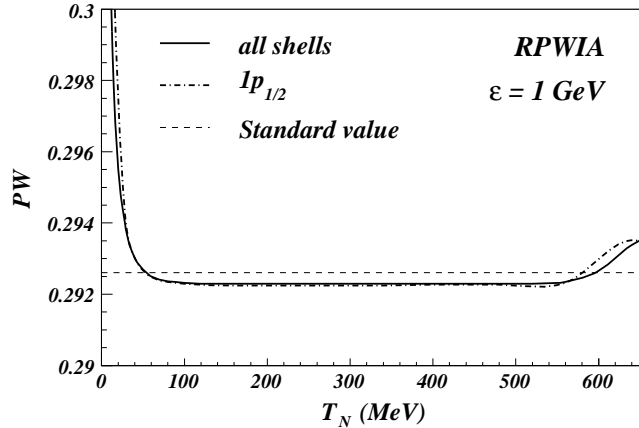


FIG. 1: The RPWIA Paschos-Wolfenstein relation as a function of the outgoing nucleon's kinetic energy T_N for an incoming neutrino energy of 1 GeV and an ^{16}O target nucleus (full line). Shown separately is the contribution of the $1p_{1/2}$ shell (dash-dotted). The dashed line represents the analytic value derived in Eq. (23), with $\sin^2 \theta_W = 0.2224$ and $\cos \theta_c = 0.974$.

from the total, shell-summed expression. Both curves show a remarkably constant behavior over a broad T_N interval and are in excellent agreement with the analytic value in Eq. (23). At very small T_N values, threshold effects induce large deviations. The sudden increase near $T_N \approx 550$ MeV relates to a decrease of the corresponding neutrino-induced NC and CC cross sections at the same energy, as shown in Fig. 2. For an incoming neutrino energy of 1 GeV, nuclear binding effects do not seem to influence the PW relation considerably. As can be appreciated from Fig. 1, Eq. (23) provides a very good approximation under those circumstances. In Fig. 3, we studied the sensitivity to the adopted parameterization for the electroweak form factors. Employing the *updated* BBA-2003 parameterization [30] for the weak vector form factors apparently yields no difference with respect to the usual dipole form. Indeed, the fact that the results in Figs. 1 and 3 are relatively T_N independent indicates that the Q^2 dependence is largely cancelled out in the PW ratio. Accordingly, the sensitivity to the adopted Q^2 evolution of the form factors is minor. An interesting by-product of this feature is that the PW relation does not depend on the axial form factor's cut-off mass M_A , which constitutes a possible source of uncertainty in the determination of g_A^s from neutrino cross-section ratios [25, 26]. Similarly, Fig. 3 shows that the use of a

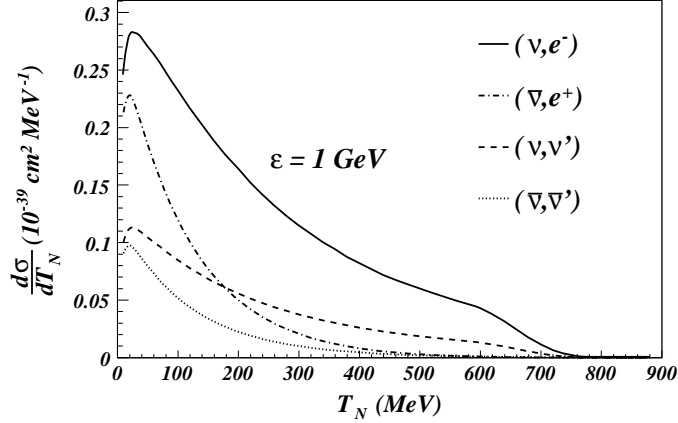


FIG. 2: ^{16}O differential cross sections for an incoming (anti)neutrino energy of 1 GeV. The full (dash-dotted) line represents the (anti)neutrino CC cross section, while the dashed (dotted) line depicts the (anti)neutrino NC cross section.

different prescription for the weak one-nucleon current operator exercises only the smallest of influences on the PW relation.

Most neutrino experiments, however, do not possess the discriminative power to measure

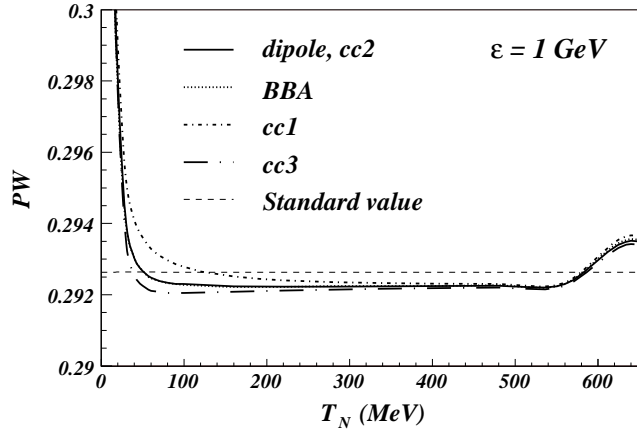


FIG. 3: The RPWIA Paschos-Wolfenstein relation as a function of T_N for the ^{16}O $1p_{1/2}$ shell and an incoming neutrino energy of 1 GeV. The reference curve, with dipole vector form factors and the $cc2$ prescription for the one-nucleon vertex function, is drawn as a full line. Using the BBA-2003 parameterization results in the dotted curve. The (long) dash-dotted curve is obtained with the ($cc3$) $cc1$ prescription. The dashed line represents the analytic value of Eq. (23).

the ejectile's kinematics. A comparison with experimental results is facilitated using total

cross sections, summed over all final states of the outgoing nucleon. Hence, it is useful to evaluate the integrated expression

$$PW_{int} = \frac{\sigma^{NC}(\nu A) - \sigma^{NC}(\bar{\nu} A)}{\sigma^{CC}(\nu A) - \sigma^{CC}(\bar{\nu} A)}, \quad (24)$$

obtained by integrating $d\sigma/dT_N$ over T_N . Figure 4 displays PW_{int} for $\nu/\bar{\nu}$ - ^{16}O cross sections and various incoming neutrino energies ranging from 100 MeV to 2 GeV. From $\epsilon = 500$

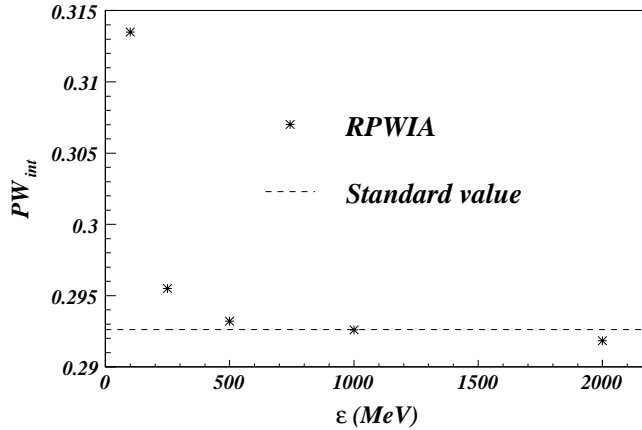


FIG. 4: Paschos-Wolfenstein relation for total $\nu/\bar{\nu}$ - ^{16}O cross sections against incoming neutrino energy. The dashed line represents the standard value.

MeV onwards, the calculated values agree with the standard value at the 0.5 percent level, illustrating once more the validity of the approximation of Eq. (23) in the relativistic plane-wave approximation. However, large discrepancies are observed at lower incoming energies. There, binding effects play an important role in the relative magnitude of the individual shell contributions to the cross sections. As a result, the expressions in numerator and denominator of Eq. (22) do not cancel entirely, thereby shifting PW_{int} to larger values. With increasing incoming neutrino energies, differences between the contributions of different shells become of less importance and the numerically computed PW values take on the value for the free nucleon.

In several experiments, ν_μ and $\bar{\nu}_\mu$ beams are employed. Consequently, the outgoing-muon's mass needs to be taken into account when calculating the CC cross sections. For sufficiently high muon-neutrino energies, however, it is readily seen that the mass of the muon (≈ 105.7 MeV) hardly influences the T_N dependence of the CC cross sections. Indeed, the nuclear responses should not be different, since a final nucleon state of fixed kinetic energy

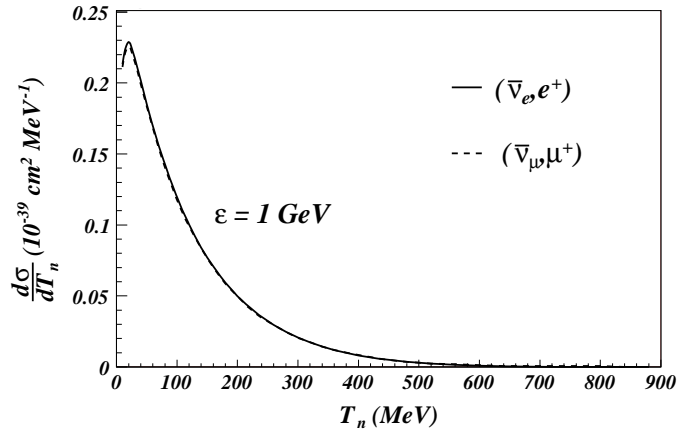


FIG. 5: Antineutrino-induced CC differential cross sections for ^{16}O as a function of the outgoing neutron's kinetic energy T_n . The full (dashed) line corresponds to an outgoing positron (antimuon).

must be created, irrespective of the outgoing lepton's nature. As for the kinematic factors (Table I), to a very good approximation the expression $\zeta = \sqrt{1 - \frac{M_l^2}{\epsilon^2}}$ equals 1 for electrons. For sufficiently high incoming energies, $\zeta \approx 1$ also holds for muon neutrinos. Figure 5 indicates that this reasoning is already valid for an incoming $\bar{\nu}_\mu$ energy of 1 GeV.

B. Final-state interactions

Unavoidably connected with the nucleon knockout channel under consideration, is the nuclear effect stemming from the ejectile searching its way through the residual nucleus. Here, these final-state interactions are modelled by a relativistic multiple-scattering Glauber approximation (RMSGGA), introduced in Section III. In this Glauber model, FSI roughly halve the cross sections for ^{16}O . As the PW relation takes ratios of cross sections, FSI effects cancel to a large extent, which is shown in Fig. 6 for an incoming neutrino energy of 1 GeV. To better illustrate the influence of FSI mechanisms, a $\pm 1\%$ error on the standard PW value is indicated. In the region where the RMSGGA produces valid results, i.e. for T_N down to 200 MeV [22], FSI mechanisms increase the computed PW ratio by less than one percent.

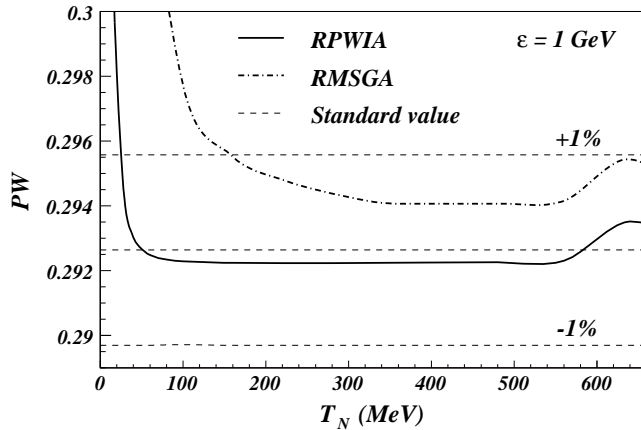


FIG. 6: The Paschos-Wolfenstein relation as a function of T_N for the ^{16}O $1p_{1/2}$ shell. The full (dash-dotted) line shows the RPWIA (RMSGGA) case. The dashed lines represent the standard PW value, with errors of 1%.

C. Neutron excess

In the preceding subsections, the PW relation was investigated for a target with an equal number of protons and neutrons. For sufficiently high energies, the balance between protons and neutrons make the $\sin^2 \theta_W$ dependence of the PW relation the traditional one of Eq. (4). Evidently, neutrino-scattering experiments often employ heavier target nuclei, with an excess amount of neutrons. The additional energy-dependent terms that are introduced in the PW formula will affect the predicted PW standard value (23), which required the perfect cancellation between proton and neutron contributions. Figure 7 shows the T_N dependence of the PW relation for ^{56}Fe at an incoming neutrino energy of 1 GeV. The specific energy dependence of PW in the iron case is given shape by the extra ν -induced CC cross sections in the denominator. Thereby, low PW values correspond with the peak region and high values with the tail of the excess neutrons' contribution to $\sigma^{CC}(\nu A)$. In general, the neutron excess in the iron target lowers PW values by $\gtrsim 10\%$. Correspondingly, of all nuclear effects looked into here, the neutron-excess correction to the PW relation is the largest and most important one.

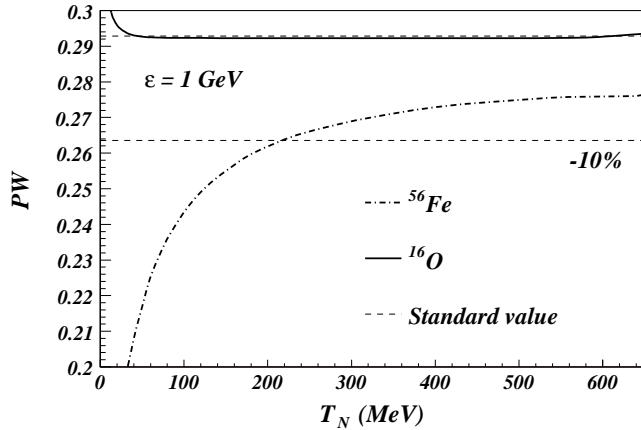


FIG. 7: The RPWIA Paschos-Wolfenstein relation as a function of T_N for an iron target (dash-dotted). Other notations refer to Fig. 1. For reference purposes, a dashed-line denoting the 10%-reduced standard PW value is added.

D. Model dependence and $\sin^2 \theta_W$ determination

Of course, to be relevant for future neutrino-scattering experiments, the above predictions need to be discussed in terms of their model dependence. To this end, we follow the line of reasoning in Refs. [24, 26], where the difference between cross sections provided by a relativistic Fermi-gas model (RFG) and a relativistic shell model (RSM) is assumed to be indicative of the theoretical model uncertainty itself. While sizeable for separate cross sections at lower incoming neutrino energies, nuclear-model dependences already seem to vanish at $\epsilon = 1$ GeV where the RSM curves coincide with the RFG ones [24]. A similar conclusion is reached in [22], where a comparison is made between RPWIA shell-model cross sections and RFG results. As the neutrino energy increases to 1 GeV, the RFG curves approach more and more the RPWIA predictions. In the same work, two methods to incorporate FSI mechanisms were compared: the Glauber approach also applied here and the relativistic optical potential approximation. At $\epsilon = 1$ GeV, both techniques were found to produce similar results down to remarkably low nucleon kinetic energies $T_N \sim 200$ MeV. Hence, as nuclear-model uncertainties seem to be negligible at $\epsilon = 1$ GeV for separate cross sections, we conclude that the PW relation, a superratio, mitigates these model dependences well below the level of all other nuclear effects studied in this work.

For isoscalar target nuclei and energetic neutrinos, the whole of nuclear-model uncertainties

on the PW relation is seen to be well within percentage range. Evidently, this means that a PW measurement with percent-level accuracy can only resolve non-isoscalar nuclear effects. Notwithstanding the extreme stability with respect to theoretical uncertainties in nuclear modelling, a quick glance at the PW relation’s Weinberg-angle sensitivity (from Eq. (4))

$$\frac{\Delta\text{PW}}{\text{PW}} = \frac{-\Delta \sin^2 \theta_W}{\frac{1}{2} - \sin^2 \theta_W}, \quad (25)$$

immediately qualifies any ambition to exploit the PW relation as an electroweak precision tool. From Eq. (25), a $\pm 1\%$ theoretical uncertainty on the PW relation would result in an equally large *nuclear-model error* on the Weinberg angle $\Delta_{nuc}(\sin^2 \theta_W) = \mp 0.0028$. On the contrary, a 10% measurement error for the parity-violating asymmetry A_{PV} in $\vec{e}\vec{e}$ Møller scattering at $Q^2 = 0.026 \text{ GeV}^2$ translates in a 1% uncertainty on the corresponding Weinberg-angle value [12]. The newly proposed Qweak experiment at Jefferson Lab aims at a 4% measurement of the proton’s weak charge Q_w^p , resulting in a 0.3% measurement of $\sin^2 \theta_W$ [32]. In this type of experiments, the sensitivity to the weak mixing angle is substantially enhanced by the factor $1/4 - \sin^2 \theta_W$ figuring in the A_{PV} expression. Obviously, the PW relation cannot compete with the level of sensitivity achievable in this sector and is therefore less suited as an electroweak precision test.

E. Strangeness

As a final point, we discuss the impact of the nucleon’s strangeness content on the PW relation. State-of-the-art reviews addressing the experimental progress on strange electromagnetic form factors and the strangeness contribution to the nucleon’s spin can be found in Refs. [33] and [34] respectively. Generally speaking, PVES experiments show a tendency towards small, positive values for the strangeness magnetic moment μ_s [33, 35, 36]. Leptonic DIS experiments seem to suggest a value of ≈ -0.1 for g_A^s [34]. As baseline strangeness parameter values, we therefore adopt predictions from the chiral quark-soliton model (CQSM) with kaon asymptotics [37], namely $\mu_s = 0.115$ and $g_A^s = -0.075$. We wish to stress that the available strangeness information still exhibits relatively large error flags. Moreover, there exist fundamental discrepancies between the experimentally favored positive μ_s and most model predictions [33, 38]. So, the values used here can be regarded as a model prediction for μ_s and g_A^s which is compatible with currently available data. Figure 8 illustrates the

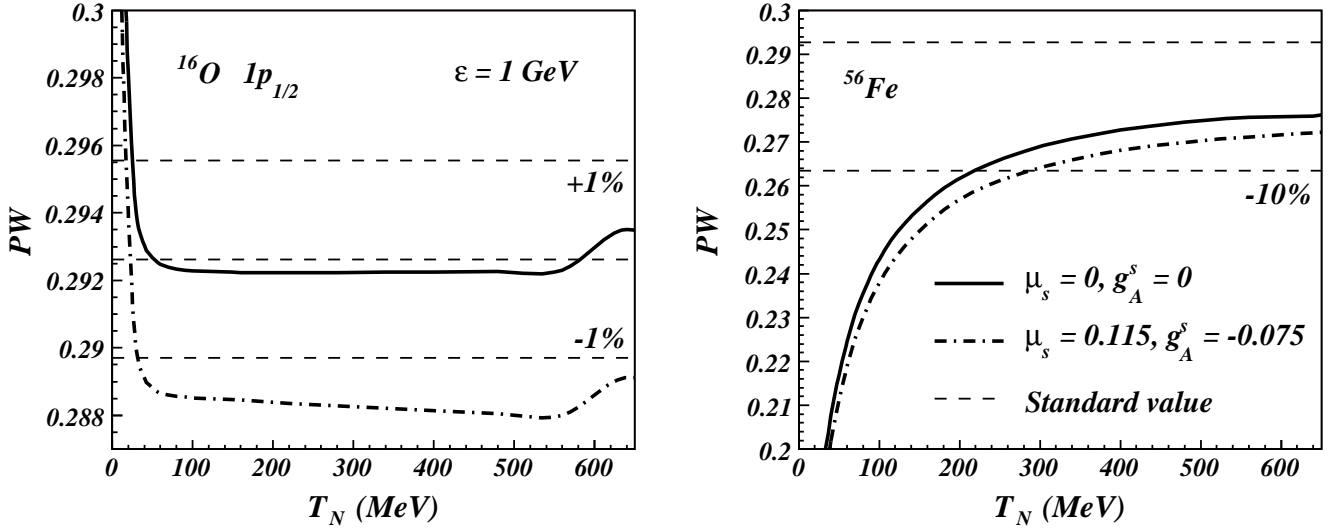


FIG. 8: The left (right) panel shows the RPWIA Paschos-Wolfenstein relation for the $^{16}\text{O } 1p_{1/2}$ shell (an ^{56}Fe target nucleus) and a 1 GeV incoming neutrino energy. Full (dash-dotted) lines correspond to $g_A^s = \mu_s = 0$ ($g_A^s = -0.075, \mu_s = 0.115$). For comparison, the standard PW values without strangeness are included (dashed lines).

influence of non-zero strangeness parameters on the PW relation. As can be observed from the left panel, the inclusion of strangeness alters the PW relation for an isoscalar target by an amount of $\sim 1\%$. For ^{56}Fe , a nucleus with neutron excess, the effect is larger ($\sim 2\%$). Summing over an equal number of proton and neutron contributions effectively cancels all isovector-strangeness interference terms, thereby reducing the PW relation to the analytic estimate (23). On the contrary, the extra neutrons in ^{56}Fe skew this proton-neutron balance, producing a larger deviation from the PW relation without strangeness. Clearly, strangeness adds a significant amount of uncertainty when attempting to determine $\sin^2 \theta_W$ from the PW relation. A simple way of visualizing the mutual influence of the parameters entering the PW relation is by considering the correlation plots in Fig. 9. We took Eq. (23) with the baseline parameter values as a starting point to calculate the lines of constant PW. From the left panel of Fig. 9, one can infer that a 50% uncertainty on g_A^s translates in a 0.7% error on $\sin^2 \theta_W$ if we assume that everything else is known. On the other hand, extracting $\sin^2 \theta_W$ from the PW relation is visibly less sensitive to the value of μ_s , yielding only a +0.3% increase if μ_s is changed from 0.115 to 0. Again, it emerges that the limited information on g_A^s and μ_s presently at hand, does not allow one to exploit the PW relation to probe the

Weinberg angle with the sensitivity achievable in PVES. Turning things around, however,

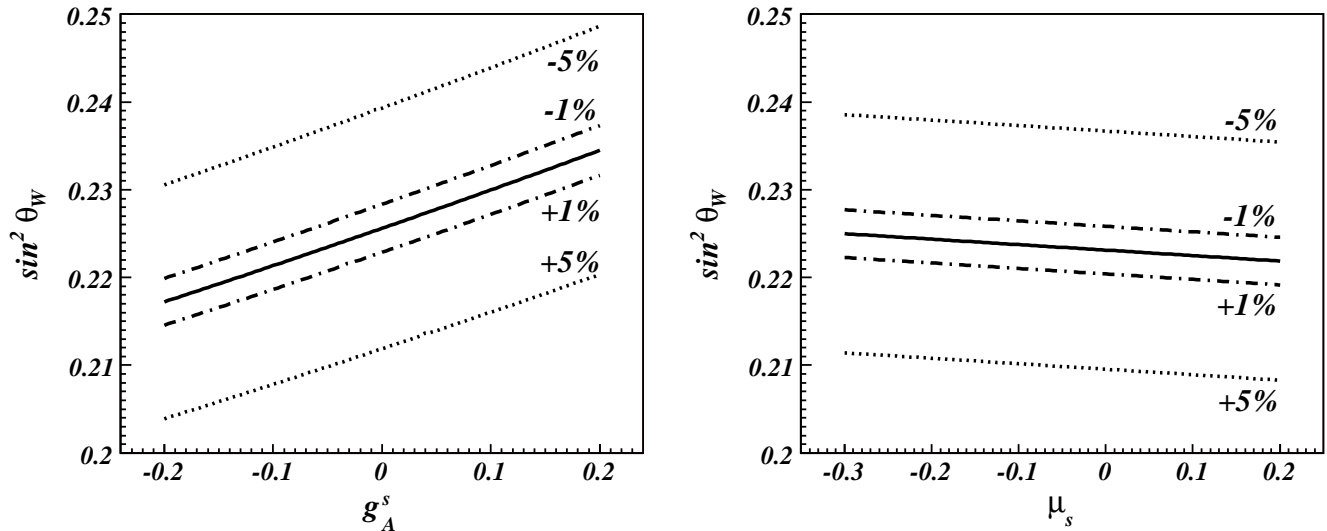


FIG. 9: Plots showing how $\sin^2 \theta_W$ and strangeness parameter values are correlated in the PW relation. The full line corresponds to values of the indicated parameters for which the PW relation is constant. The dash-dotted (dotted) lines have the same meaning, but with PW equal to $\pm 1\%$ ($\pm 5\%$) the full-line value.

a precisely known Weinberg-angle value may turn out valuable in trying to pin down g_A^s from a measurement of the QE PW relation. Ratios of neutrino-induced cross sections are indeed considered useful for studying the strangeness content of the nucleon, and notably the strangeness contribution to the nucleon's spin g_A^s . Well-covered examples are the ratio of proton-to-neutron NC reactions [24, 26, 39], NC to CC cross-section ratios [40, 41], polarization asymmetries [38] and the Paschos-Wolfenstein relation for proton knockout PW_p [24]. In the latter article, PW_p was seen to have a strong dependence on g_A^s . In addition, results presented in this work justify the optimism about a model-independent g_A^s determination [25] by measuring PW_p in the right circumstances, i.e. with an isoscalar target nucleus and an incoming neutrino energy of about 1 GeV. To study how the finite precision on $\sin^2 \theta_W$ and μ_s influences the accuracy with which g_A^s can be extracted from PW_p , we consider the correlation plots in Fig. 10. The curves were again drawn from Eq. (23), now retaining only the proton contribution in the numerator ($\tau_3 = +1$) to obtain lines of constant PW_p . From this figure, we see that a 5% measurement of PW_p results in a ± 0.067 determination of g_A^s . For comparison, the FINeSSE collaboration aims at a 6% measurement of the NC/CC

ratio down to $Q^2 = 0.2 \text{ GeV}^2$, corresponding to a ± 0.04 measurement of g_A^s . The left panel in Fig. 10 learns that a 1% uncertainty on $\sin^2 \theta_W$ gives rise to a 20% uncertainty on g_A^s , assuming again that everything else is fixed. The inconclusive information on μ_s available at present has a far more severe effect on the value of g_A^s , as can be derived from the right panel. Shifting the strangeness magnetic moment from 0.115 to 0, g_A^s changes by ~ 0.07 . We recall that nuclear-model uncertainties can be mitigated to the 1% level, corresponding to $\Delta_{nuc}(g_A^s) \sim 0.015$. This analysis stresses the importance of further experimental efforts to put more stringent limits on the strangeness form factors of the nucleon. As apparent from this PW_p case, experiments in the vector and axial-vector sector heavily depend on each other in the sense that both types of measurements need reliable input values for the other strangeness parameters.

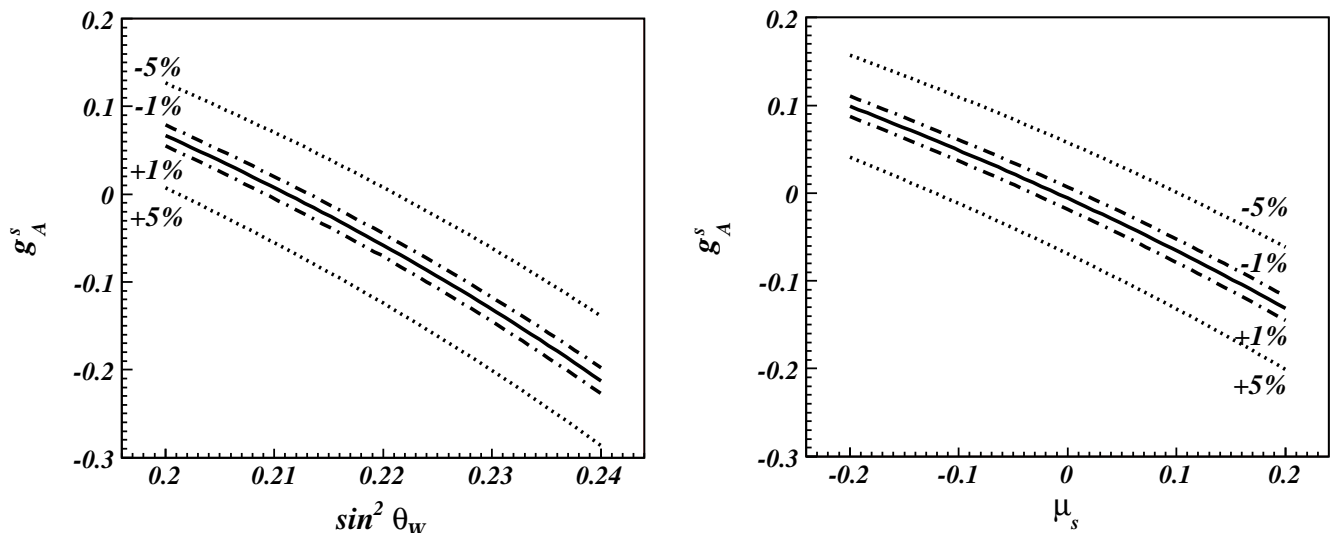


FIG. 10: Correlation plots showing how the axial strangeness parameter g_A^s is intertwined with $\sin^2 \theta_W$ (left) and μ_s (right) through the PW relation for proton knockout PW_p . The full line corresponds to values of the indicated parameters for which PW_p is constant. The dash-dotted (dotted) lines have the same meaning, but with PW_p equal to $\pm 1\%$ ($\pm 5\%$) the full-line value.

VI. CONCLUSIONS

Adopting a fully relativistic nucleon knockout model for the description of quasi-elastic neutrino-nucleus interactions, we have conducted a study of the Paschos-Wolfenstein relation

with hadronic degrees of freedom. Results are presented for ^{16}O and ^{56}Fe target nuclei and incoming neutrino energies between 100 MeV and 2 GeV. We estimate that nuclear-model uncertainties amount to a 1% theoretical error bar for the PW relation in the case of sufficiently high neutrino energies ($\gtrsim 1$ GeV) and isoscalar target nuclei. Under these conditions, the Weinberg-angle dependence of the PW relation is to a very good approximation identical to the one constructed with DIS neutrino-nucleon cross sections. Binding effects produce a sizeable shift at lower incoming neutrino energies, but become negligible beyond 500 MeV. The largest correction stems from neutron excess in the target, which drastically lowers the PW curve. Though nuclear-model effects are extremely well controlled, the PW relation is no match for electroweak precision probes in other sectors, notably PVES experiments whose sensitivity to the Weinberg angle is considerably larger. The poor information on the nucleon's strangeness content presently at hand also induces 1%-level uncertainties on the PW relation, and consequently puts even more stringent limits on its $\sin^2 \theta_W$ sensitivity. An extraction of the strangeness contribution to the nucleon's spin g_A^s through the proton knockout part of the PW relation clearly benefits from the small theoretical uncertainties involved ($\Delta_{nuc}(g_A^s) \sim 0.015$), but depends heavily on a reliable input for the strange vector form factors.

Acknowledgments

The authors acknowledge financial support from the Fund for Scientific Research (FWO) Flanders and the University Research Board (BOF).

-
- [1] S. Boyd (MINERvA), Nucl. Phys. Proc. Suppl. **139**, 311 (2005).
 - [2] S. Pate, Eur. Phys. J. A **24S2**, 67 (2005).
 - [3] FINeSSE proposal, L. Bugel et al. (FINeSSE), hep-ex/0402007.
 - [4] G. P. Zeller et al. (NuTeV), Phys. Rev. Lett. **88**, 091802 (2002).
 - [5] A. B. Balantekin, J. H. de Jesus and C. Volpe, Phys. Lett. **B634**, 180 (2006).
 - [6] J. M. Conrad, J. M. Link and M. H. Shaevitz, Phys. Rev. D **71**, 073013 (2005).
 - [7] A. Czarnecki and W. J. Marciano, Phys. Rev. D **53**, 1066 (1996).
 - [8] J. Erler and M. J. Ramsey-Musolf, Phys. Rev. D **72**, 073003 (2005).

- [9] G. Abbiendi et al. (OPAL), Phys. Lett. **B546**, 29 (2002).
- [10] K. Abe et al. (SLD), Phys. Rev. Lett. **86**, 1162 (2001).
- [11] A. Derevianko, Phys. Rev. Lett. **85**, 1618 (2000).
- [12] P. L. Anthony et al. (SLAC E158), Phys. Rev. Lett. **95**, 081601 (2005).
- [13] G. P. Zeller et al. (NuTeV), Phys. Rev. D **65**, 111103 (2002).
- [14] K. P. O. Diener, S. Dittmaier and W. Hollik, Phys. Rev. D **69**, 073005 (2004).
- [15] K. J. Eskola and H. Paukkunen, JHEP **0606**, 008 (2006).
- [16] S. A. Kulagin, Phys. Rev. D **67**, 091301 (2003).
- [17] A. Kurylov, M. J. Ramsey-Musolf and S. Su, Nucl. Phys. **B667**, 321 (2003).
- [18] S. Davidson, S. Forte, P. Gambino, N. Rius and A. Strumia, J. High Energy Phys. **02**, 037 (2002).
- [19] R. N. Mohapatra et al., hep-ph/0510213 (2005).
- [20] E. A. Paschos and L. Wolfenstein, Phys. Rev. D **7**, 91 (1973).
- [21] J. G. Morfin, Nucl. Phys. Proc. Suppl. **149**, 233 (2005).
- [22] M. C. Martínez, P. Lava, N. Jachowicz, J. Ryckebusch, K. Vantournhout and J. M. Udías, Phys. Rev. C **73**, 024607 (2006).
- [23] T. W. Donnelly, M. J. Musolf, W. M. Alberico, M. B. Barbaro, A. De Pace and A. Molinari, Nucl. Phys. **A541**, 525 (1992).
- [24] W. M. Alberico, M. B. Barbaro, S. M. Bilenky, J. A. Caballero, C. Giunti, C. Maieron, E. Moya de Guerra and J. M. Udías, Nucl. Phys. **A623**, 471 (1997).
- [25] W. M. Alberico, M. B. Barbaro, S. M. Bilenky, J. A. Caballero, C. Giunti, C. Maieron, E. Moya de Guerra and J. M. Udías, Nucl. Phys. **A651**, 277 (1999).
- [26] W. M. Alberico, M. B. Barbaro, S. M. Bilenky, J. A. Caballero, C. Giunti, C. Maieron, E. Moya de Guerra and J. M. Udías, Phys. Lett. **B438**, 9 (1998).
- [27] M. B. Barbaro, A. De Pace, T. W. Donnelly, A. Molinari and M. J. Musolf, Phys. Rev. C **54**, 1954 (1996).
- [28] C. Maieron, Acta Phys. Pol. B **37**, 2287 (2006).
- [29] G. P. Zeller, Ph.D. Thesis, Northwestern University, 2002.
- [30] H. Budd, A. Bodek and J. Arrington, hep-ex/0308005.
- [31] J. Ryckebusch, D. Debruyne, P. Lava, S. Janssen, B. Van Overmeire and T. Van Cauteren, Nucl. Phys. **A728**, 226 (2003).

- [32] D. S. Armstrong et al. (Qweak), *Eur. Phys. J. A* **24S2**, 155 (2005).
- [33] M. J. Ramsey-Musolf, *Eur. Phys. J. A* **24S2**, 197 (2005).
- [34] S. F. Pate, *Eur. Phys. J. A* **24S2**, 67 (2005).
- [35] D. S. Armstrong et al. (G0), *Phys. Rev. Lett.* **95**, 092001 (2005).
- [36] K. A. Aniol et al. (HAPPEX), *Phys. Lett.* **B635**, 275 (2006).
- [37] A. Silva, D. Urbano, H.-C. Kim and K. Goeke, *Eur. Phys. J. A* **24S2**, 93 (2005).
- [38] P. Lava, N. Jachowicz, M. C. Martínez and J. Ryckebusch, *Phys. Rev. C* **73**, 064605 (2006).
- [39] G. Garvey, E. Kolbe, K. Langanke and S. Krewald, *Phys. Rev. C* **48**, 1919 (1993).
- [40] B. I. S. van der Ventel and J. Piekarewicz, *Phys. Rev. C* **73**, 025501 (2006).
- [41] A. Meucci, C. Giusti and F. D. Pacati, *Nucl. Phys.* **A773**, 250 (2006).